

Global Numerical Model For Orifice and Insert Region of a Lanthanum Hexaboride Thermionic Hollow Cathode

Oguz Korkmaz*, Murat Celik†
Bogazici University, Istanbul, 34342, Turkey
oguzkorkmaz89@gmail.com

SP2014_2979704

Thermionic hollow cathode is an indispensable component for the applications which require electrons. This device has been used in wide variety of areas such as spacecraft electric propulsion systems, material processing, lasers. Especially in electric propulsion systems, hollow cathodes are being used as electron source for propellant ionization and beam neutralization. Moreover, it is also a promising candidate for utilization as propulsion system in microsattellites or nanosatellites due to its small physical volume. On the other hand, the small geometry of it makes the plasma diagnostics difficult to perform which is why numerical studies become important in order to understand the driving physical processes behind its operation. In this paper, a global numerical model for the insert and orifice plasma of a hollow cathode is presented. In the present model, it is assumed that the properties of the plasma both in the orifice and insert regions are volume-averaged. The results of this preliminary study show that it is a promising modelling tool for orificed hollow cathodes since general tendency in the properties of the insert and orifice plasmas against the changes in operation conditions and geometry is captured.

Nomenclature

A_{emit}	= Insert effective emission area	[m ²]
r_e	= Insert radius	[m]
L_{emit}	= Insert effective emission length	[m]
r_o	= Orifice radius	[m]
d_o	= Orifice diameter	[m]
n_e	= Insert region plasma density	[m ⁻³]
n_o	= Orifice region plasma density	[m ⁻³]
N_e	= Insert region plasma neutral density	[m ⁻³]
N_o	= Orifice region plasma neutral density	[m ⁻³]
ϕ_{wf}	= Work function of the insert material	[V]
P	= Pressure	[Torr]
R_g	= Specific gas constant of propellant	[J/kgK]
$T_{eV,ins}$	= Insert region plasma electron temperature	[eV]
$T_{e,ins}$	= Insert region plasma electron temperature	[K]
ζ	= Viscosity	[Poise]
\dot{m}	= Propellant flow rate	[mg/s]
Q	= Propellant flow rate	[sccm]
$T_{w,ins}$	= Insert wall temperature	[K]
$T_{w,orf}$	= Orifice wall temperature	[K]
U_i	= First ionization energy of propellant	[eV]
γ	= Specific heat ratio of propellant	

*M.S. Student, Mechanical Engineering, Bogazici University.

†Assistant Professor, Mechanical Engineering, Bogazici University.

I. Introduction

Thermionic hollow cathodes have been used for more than 50 years in wide variety of applications. In ion and Hall thrusters, ionization of neutral propellant atoms through both electron impact and step-wise ionization and neutralization of ion beam to prevent spacecraft charging require electrons. Hence, installation of a particular device which can release electrons is a must for these systems to work. Due to its small physical volume, simple geometry and ease of operation, thermionic hollow cathodes have been used in these and many other devices for years.

Orificed hollow cathodes (OHC) that are used in electric propulsion systems typically consist of a thin, long, hollow cylindrical refractory metal tube in which an insert material with a low work function is placed. A schematic of a hollow cathode is shown in Figure 1. Orifice, a refractory metal, is welded at the downstream end. The reason of orifice utilization in OHC is to maintain high internal pressure, on the order of $10^3 - 10^4$ Pa. Moreover, orifice also contributes to heating of the emitter material. The electron release from insert material with thermionic emission is an important phenomenon which can determine the power consumption and operation parameters of hollow cathode. Work function, evaporation rate and poisoning resistance against the impurities in the propellant are important parameters for emitter material selection. Barium-Oxide impregnated tungsten ($\text{BaO} - \text{W}$) and Lanthanum hexaboride (LaB_6) are most common materials used as thermionic emitter in OHC. $\text{BaO} - \text{W}$ material has work function around 1.6 eV and can emit electrons under 1000°C . However, this material can easily be poisoned. For this reason, high purity propellant usage is an extreme importance in order to ensure high lifetime in OHC. LaB_6 , on the other hand, is resistant against poisoning and it also has low evaporation rate. This emissive material was first discovered by Lafferty [1]. Its high thermal conductivity ensures uniform temperature distribution on the insert surface [2]. The work function of this material is around 2.67 eV [3]. Due to the fact that LaB_6 has higher work function than $\text{BaO} - \text{W}$ material, it requires higher temperature to give same amount of current density. Apart from its high work function, another shortcoming of LaB_6 is that rapid cooling and heating causes it to fracture. The supportive material of LaB_6 should also be chosen cautiously because it reacts with many refractory materials such as tungsten, molybdenum. Since thermal properties of graphite is similar to those of LaB_6 and it does

not react with LaB_6 , it is a good option to be used as supporting material [4], [5].

There is also a cylindrical keeper tube which is mounted around the cathode tube. Main function of the keeper is to create an attracting potential difference for electrons. At initiation stage of hollow cathode, this potential difference is used to accelerate thermionically emitted electrons in order to make them have enough energy to ionize the neutral propellant atoms. The neutral propellant atoms injected from upstream end of hollow cathode, experience collision with primary electrons when they reach insert region. As a result, a dense plasma environment is created in the emitter region. After system reaches steady state, keeper is used to regulate the electron discharge. In addition, keeper protects the cathode assembly from ion bombardment coming from thruster plasma. Another task of the keeper is to maintain high insert temperature [6].

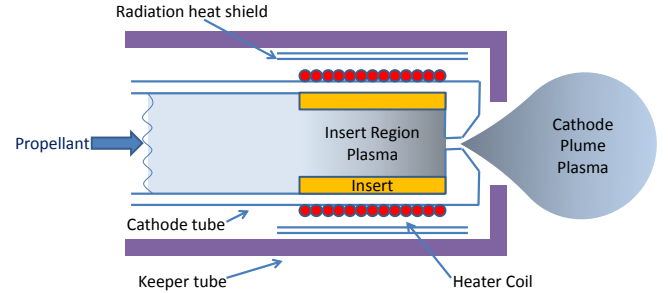


Figure 1: Schematic of a hollow cathode

Heater coils, wrapped around the insert region of the cathode tube, are mostly made of refractory metals such as tantalum. The heater supplies the necessary amount of heat to increase the temperature of the emitter material to its emission temperature. As mentioned earlier, utilization of low work function insert can minimize the power consumption of heater, and thus power consumption of hollow cathode. A radiation shield is also placed between heater and keeper in order to minimize the energy loss due to radiation. The heater is turned off after the system becomes self-sustained [7]. After this point on, the amount of heat which is essential for continuation of electron release from emitter is supplied by heat conduction from orifice and bombardment of insert surface with ions and electrons coming from insert plasma [8],[9]. In order for the electrons to reach the insert surface, they must have enough energy to overcome the reverse potential present at the cathode sheath. The thickness of this sheath is on the order of several Debye lengths. The presence of an electric field at the cathode sheath reduces the experimentally found work function of the emitter material as well.

II. Hollow Cathode Global Model

The main goal of the model is to assess the cathode for different geometry and operating conditions. In this model, it is assumed that quasi-neutral plasma with uniform plasma parameters (electron density, electron temperature, neutral density etc.) is present in both emitter and orifice region. The plasma in both regions is considered as if it is a combination of thermalized electrons, singly-charged ions and neutrals and it is enclosed within a cylindrical control volume. The model considers that the particles in the orifice and insert plasma have Maxwellian distribution. The collisions occurring in the plasma cause the particles to deviate from their Maxwellian distribution however within the time between collision they again relax to their Maxwellian distribution. During the modelling, it is assumed that the heavy particles (neutrals and ions) are at the same temperature with the cathode wall. Ion conservation and plasma energy balance equations are solved with an iterative procedure until current balance equation written for insert plasma and surface energy balance written for orifice wall are satisfied. The work presented here follows the previous studies of different researchers [8], [10], [11]. The wall temperature of the insert and orifice was varied until the insert current balance and orifice surface energy balance is satisfied. Throughout the iterations, ion conservation and plasma energy balance equations are solved using bisection method in order to obtain electron temperature and plasma density.

Emitter Model

Ion conservation, plasma energy balance and insert current balance equations are written for the emitter region. As depicted in Figure 2, the ion loss mechanism in this region is the thermal flux toward the cathode base and the strike of ions to the insert surface and orifice wall. The ions passing through the sheath on the insert gain Bohm velocity and hit the surface of the insert material and orifice wall. The ion generation mechanism, on the other hand, is ion production due to the electron impact ionization. The ion conservation equation of emitter region plasma in steady-state operation is given as follows:

$$q\pi r_e^2 L_{emit} N_e n_e \langle \sigma v_e \rangle = J_{i,th} (\pi r_e^2) + J_{i,Bohm} (2\pi r_e L_{emit} + \pi r_e^2 - \pi r_o^2) \quad (1)$$

The left hand-side of the Equation (1) represents the amount of ion produced by electron impact ion-

ization. The first term on the right hand side stands for the thermally lost ions to upstream and the second term shows the ion loss to the insert surface and orifice wall. The ionization rate function, as a function of electron temperature, T_{eV} , is calculated according to the expression given in [8]. Even though, it is speculated by [12] and experimentally observed by [13] that a double layer is formed at the constriction between insert and orifice region plasma, it is not taken into account in Equation (1).

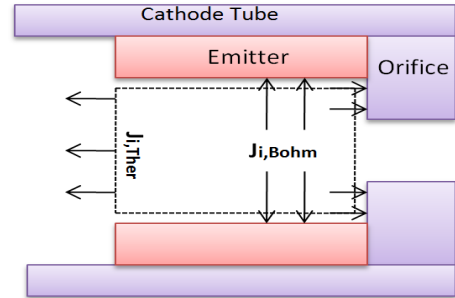


Figure 2: Mobility of ions in the emitter region

Apart from ion conservation, energy balance equation of the emitter plasma is also solved. The energy balance for the insert region plasma involves all the energy that comes in and out of the plasma region. In the insert region of the hollow cathode, the energy gain of the plasma due to ohmic heating and thermionic electron emission is balanced by the energy loss due to ions leaving the control volume, random electron current to the insert surface and electron discharge current. In energy balance equation, it is considered that the plasma is optically thick enough, so that radiated energy is again absorbed by the plasma. Thus, radiation losses are not considered. Energy removed via excitation is also ignored [8]:

$$I_{em}\phi_s + R_e I_d^2 = I_{i,out} \left(U_i + \frac{2k_B T_{w,ins}}{q} \right) + (2T_{eV,ins} + \phi_s) I_r + \frac{5}{2} T_{eV,ins} I_d \quad (2)$$

Here I_{em} represents the thermionic emission current in Amperes, ϕ_s represents the sheath voltage built in plasma in Volts, R_e is the resistance of the plasma in Ohms, I_d is the current extracted from the cathode in Amperes, $I_{i,out}$ is the ion current out of the control volume in Amperes, U_i is the first ionization energy of xenon in eV, T_{eV} is electron temperature in eV, and I_r is the random electron current to the insert surface in Amperes at the insert region [8].

$I_{em}\phi_s$ term represents the energy input by thermionically emitted electrons that are accelerated by sheath plasma potential. $R_e I_d^2$ term repre-

sents the energy lost by the electrons to the plasma due to collisions with the ions and the neutrals in the plasma. First term on the right hand side accounts for the energy lost due to the ions leaving the control volume. $(2T_{eV} + \phi_s)I_r$ term represents the energy that is drawn from the plasma as the electrons overcome the sheath potential at the sheath edge and reaches the insert wall. $\frac{5}{2}T_{eV}I_d$ term is the energy spent to energize the extracted current. Here $3/2$ of this represents total kinetic energy in three degrees of freedom ($x, y, z, 1/2$ each) and 1 comes from work done on the electrons by pressure. As the current is extracted, this energy is carried away.

In order to calculate emitter plasma energy gain due to ohmic heating, the emitter plasma resistance, R_e , is found from the following expression [10]:

$$R_e = \eta \frac{r_e}{4/3r_e L_{emit}} \quad (3)$$

where L_{emit} is the length of the actively emitting region of the emitter, also corresponding conduction length of the plasma, r_e is the radius of the emitter region plasma, η is the resistivity of the insert region plasma. It is assumed that most of the current is carried in radial direction, thus for the current conduction an average cross-sectional area is used as given in [10]. The resistivity of the plasma is given by:

$$\eta = m_e \frac{\nu_{ei} + \nu_{en}}{q^2 n_e} \quad (4)$$

where n_e is emitter plasma density, q is the electron charge, ν_{ei} and ν_{en} are electron-ion and electron-neutral collision frequencies respectively. The electron-ion collision frequency is calculated as follows:

$$\nu_{ei} = 2.9 \times 10^{-12} \frac{n_e \ln \Lambda}{T_{eV,ins}^{3/2}} \quad (5)$$

where the quantity $\ln \Lambda$, is the Coulomb logarithm and it is given as:

$$\ln \Lambda = 23 - \frac{1}{2} \ln \left(\frac{10^{-6} n_e}{T_{eV,ins}^3} \right) \quad (6)$$

The electron-neutral collision frequency is given:

$$\nu_{en} = \sigma_{en} n_o \sqrt{\frac{8k_B T_{e,ins}}{\pi m_e}} \quad (7)$$

where σ_{en} is the electron-neutral collision cross section:

$$\sigma_{en} = 6.6 \times 10^{-19} \left[\frac{\frac{T_{eV,ins}}{4} - 0.1}{1 + \left(\frac{T_{eV,ins}}{4} \right)^{1.6}} \right] \quad (8)$$

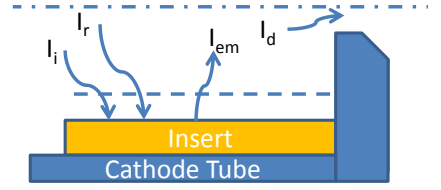


Figure 3: Schematic of the current balance in the insert region

Another equation written for emitter is the current balance. There are four currents that play part in the plasma as shown in Figure 3. In this figure the dashed line represents the sheath edge of the plasma at the insert region. The four currents that enter and leave the insert region plasma have the following relationship [8]:

$$I_{em} + I_i = I_d + I_r \quad (9)$$

In this equation, I_{em} is the amount of electron current emitted from insert with thermionic emission. Thus, I_{em} represents the total electron current leaving the insert surface and entering the insert region plasma. The thermionic current density is evaluated from Richardson-Dushman equation:

$$J_{em} = DT_{w,ins}^2 \exp \left(-\frac{q\phi_{eff}}{k_B T_{w,ins}} \right) \quad (10)$$

where D is material constant and $T_{w,ins}$ is the emitter wall temperature. D is taken as $29 \text{ Acm}^{-2} \text{K}^{-2}$ for LaB_6 [1].

In the presence of an electric field on the insert material, the apparent work function decreases. This phenomena is referred to as Schotky effect and effective work function is given as:

$$\phi_{eff} = \phi_{wf} - \sqrt{\frac{qE_s}{4\pi\epsilon_0}} \quad (11)$$

where ϕ_{wf} is the value of the work function in the literature, E_s is the electric field of the cathode sheath acting on the insert material and it is given as follows [14]:

$$E_s = \sqrt{\frac{nk_B T_{e,ins}}{\epsilon_0}} \left[2\sqrt{1 + \frac{2q\phi_s}{k_B T_{e,ins}}} - 4 \right]^{1/2} \quad (12)$$

where ϕ_s , the emitter sheath voltage drop, is given as [8]:

$$\phi_s = \frac{k_B T_{e,ins}}{q} \ln \left[\sqrt{\frac{2m_i}{\pi m_e}} \right] \quad (13)$$

The electric field caused by the sheath potential on the emitter reduces the literature work function of insert material, and thus enhances the thermionic

electron emission. Eventually, electron emission current from insert with field-enhanced thermionic emission can be calculated as follows:

$$I_{em} = J_{em}A_{emit} \quad (14)$$

I_i is the ion current that leaves the insert region plasma and reaches the surface of the emitter. These ions that reach the surface bombard the surface with their energy and contribute to the heating of the surface. I_i is calculated from Bohm sheath criterion as follows:

$$I_i = 0.61qn_e\sqrt{\frac{k_B T_{e,ins}}{m_i}}A_{emit} \quad (15)$$

where n_e is the electron density in the insert region plasma, $T_{e,ins}$ is electron temperature in K. In equation (9), I_r , the random electron current at the sheath edge, is given by:

$$I_r = \frac{1}{4}n_eq\left(\frac{8k_B T_{e,ins}}{\pi m_e}\right)^{1/2}\exp\left(\frac{-q\phi_s}{k_B T_{e,ins}}\right)A_{emit} \quad (16)$$

The neutral density in the insert region is determined by assuming Pouiselle flow through the orifice. Taking reduced temperature T_r as the ratio $T_n/289.7$. The viscosity is given by [8]:

$$\zeta = 2.3 \times 10^{-4}T_r^{0.71+\frac{0.29}{T_r}} \quad (17)$$

Then the pressure of neutral atoms will be determined in terms of Torr as follows [8]:

$$P = \sqrt{\frac{0.78Q\zeta T_r L_o}{d_o^4}} \quad (18)$$

where L_o and d_o are orifice length and diameter in cm respectively, Q is the mass flow rate in sccm. Finally, neutral density, N_o , is found from:

$$N_o = 9.65 \times 10^{24}\frac{P}{T_n} \quad (19)$$

The active emitting length of the insert depends on the discharge current, mass flow rate and orifice diameter [15]. Even though the thermal conductivity of LaB₆ is high, at high discharge currents and gas flow rates, density of the insert plasma becomes greater in the region close to the orifice [16]. Operation at high mass flow rate and discharge current elevates the temperature of the orifice. Consequently, heat flux towards insert increases and parts of the insert adjacent to the orifice get hotter. This uneven distribution of temperature on the emitter surface causes the hotter regions to emit more electrons. For determination of the effective emission length

of the insert, the simple methodology proposed by Alta group is used [17]. It is assumed that the product of the effective emission length and the insert plasma pressure is equal to 15 mPa.

Orifice Model

Similar to the emitter model, ion conservation and energy balance equations are written for orifice plasma as well. In steady state operation, there is a balance between produced ions and lost ions. The volumetric ion generation is balanced with thermal ion loss to downstream and ion loss to the orifice exit surface as shown in Figure 4.

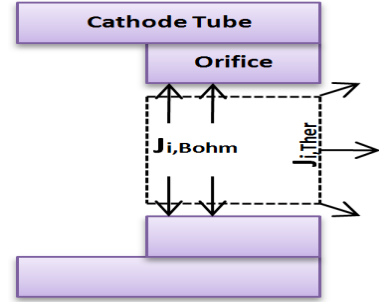


Figure 4: Mobility of ions in the orifice region

$$q\pi r_o^2 L_o N_o n_o \langle \sigma v_e \rangle = J_{Bohm,orf}(2\pi r_o L_o) + J_{th,orf}(\pi r_o^2) \quad (20)$$

Just like emitter region ion conservation equation, left hand side of Equation (20) represents the ion generation due to direct electron impact ionization and first term on the right hand side represents the amount of ion loss to the orifice wall and the second term represents the thermal ion loss out of the orifice control volume.

Orifice plasma energy balance equates the energy gain of the plasma due to resistive heating with the energy loss due to ionization and convection of electrons from orifice to insert. Since the electron temperature in the orifice is larger in comparison to the insert plasma electron temperature, the convection loss occurs. The energy equation for orifice plasma is written as follows:

$$R_o I_d^2 = (q\pi r_o^2 L_o N_o n_o \langle \sigma v_e \rangle)(U_i) + 2.5\frac{k_B}{q}I_d(T_{e,orf} - T_{e,ins}) \quad (21)$$

In Equation (21), the term on the left is the energy gain due to ohmic heating, the first term on the right is energy loss due to ionization and finally the last term is the energy loss due to electron

convection. Orifice plasma resistance is evaluated as $R_o = \eta L_o / \pi r_o^2$. Resistivity of the orifice region plasma is calculated following the same procedure explained in the previous section.

In order to calculate the neutral density in the orifice plasma, it is assumed that choked flow phenomenon occurs at the orifice exit. Under this assumption neutral density can be calculated as follows [18]:

$$N_o = \frac{\dot{m}}{M_o A_{orf} \sqrt{\gamma R_g T_{w,orf}}} \quad (22)$$

where A_{orf} represents the orifice cross sectional area, M_o is the atomic mass of xenon and \dot{m} is the propellant flow rate in terms of [kg/s].

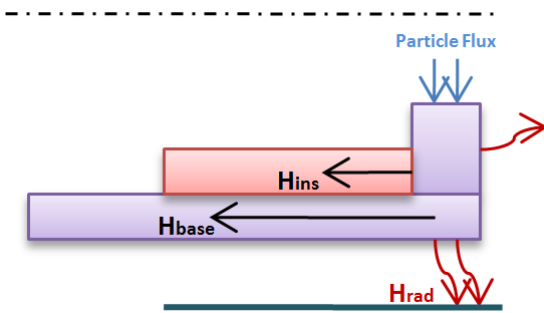


Figure 5: Orifice wall energy fluxes

Another equation written for the orifice model is the energy balance on the orifice surface. The ions passing the sheath reaches the orifice and give their energy to the orifice. Electrons striking to the orifice surface are also another energy gain mechanism. The energy loss mechanisms for the orifice is the heat conduction to the base and the insert, and thermal radiation to its surroundings. Figure 5 depicts the energy exchange in the orifice. Under these conditions, orifice wall energy balance can be written as follows:

$$I_{Bohm,orf} \left(U_i + \phi_{s,orf} + 0.5 \frac{k_B T_{w,orf}}{q} \right) + I_{r,orf} (2T_{eV,orf}) = H_{base} + H_{ins} + H_{rad} \quad (23)$$

In Equation (23), H_{base} stands for the amount of heat that is lost to base by conduction, H_{ins} represents the amount of heat that is lost to insert by conduction and H_{rad} is the amount of heat that is lost by radiation.

III. Solution of Model Equations

The reference geometry used to obtain the results are given in this section. Basically, there are three main geometric parameters that are associated with

the hollow cylindrical insert: the inner diameter, $d_{in} = 3.8$ mm, the outer diameter, $d_{out} = 6.4$ mm, the length $L_{ins} = 25$ mm. Length of the orifice and its diameter are $L_o = 0.75$ mm, $d_o = 0.75$ mm respectively. Lastly, the total length of the tungsten cathode tube must be known in order to calculate heat loss to the base $L_{tube} = 80$ mm. The thickness of the cathode tube is taken as 1 mm. The transfer coefficient of the cathode tube material and insert material must be known in order to be able to perform heat loss calculations. The thermal conductivity of insert material is taken as $k_t = 130$ W/m.K. The cathode tube is assumed to be made of tungsten, thus $k_t = 107$ W/m.K. Cathode base temperature is kept constant at 1000 K and the temperature of the shield at 1200 K during the heat transfer calculations and the variations of the thermal property of the materials due to the temperature are ignored. Since hollow cathode works in vacuum environment, there is no heat loss with conduction from insert or orifice to the radiation shield. The view factor, used in radiation heat loss calculation, is taken as unity.

For the solution of emitter region plasma, the emitter wall temperature is varied. The ion conservation equation, Equation (1), is solved using bisection method to obtain the plasma electron temperature ($T_{eV,ins}$). Insert plasma energy balance equation, Equation (2), is also solved with the same method to have the emitter plasma density (n_e). The current balance equation, Equation (9), is used as convergence criterion.

The same logic is applied for the orifice region plasma model as well. While the orifice wall temperature varies, the orifice ion conservation equation, Equation (20), and orifice plasma energy balance equation, Equation (21), is solved with bisection method in order to obtain the orifice plasma electron temperature ($T_{eV,orf}$) and density (n_o). This time, energy balance equation written on the orifice wall, Equation (23), is used as convergence criterion.

For lifetime calculation, a mathematical expression, Equation (24), is obtained for LaB₆ evaporation rate versus current density graph given in [19].

$$W = 3 \times 10^{-11} J_{em}^{(2.564)} \quad (24)$$

Lifetime of insert calculated as time required to halve the initial mass of emitter. It should be noted that this approximation for lifetime determination does not consider any other factor that can affect lifetime significantly such as poisoning.

IV. Results

Even though the calculated insert region plasma electron temperature is relatively low, the tendency with respect to discharged current is captured. As can be seen in Figure 6, the electron temperature slightly increases with increasing discharge current at a given flow rate. It is also found that the emitter plasma electron temperature is an increasing function of mass flow rate.

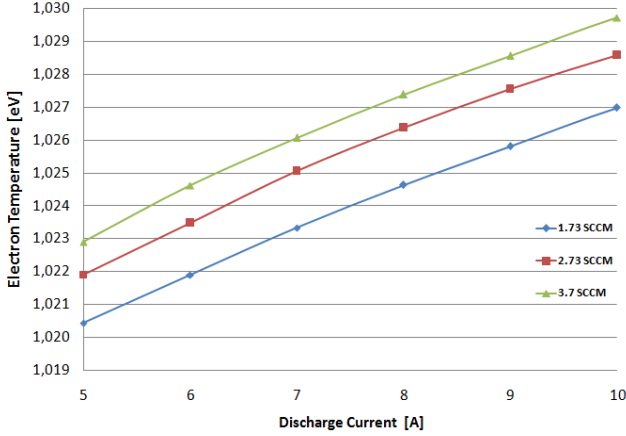


Figure 6: Emitter electron temperature as a function of discharge current

As it was shown experimentally in studies [14], [20] and [21], insert wall temperature is an increasing function of both discharge current and propellant flow rate. As can be seen in Figure 7, the emitter wall temperature increases with increasing discharge current and mass flow rate.

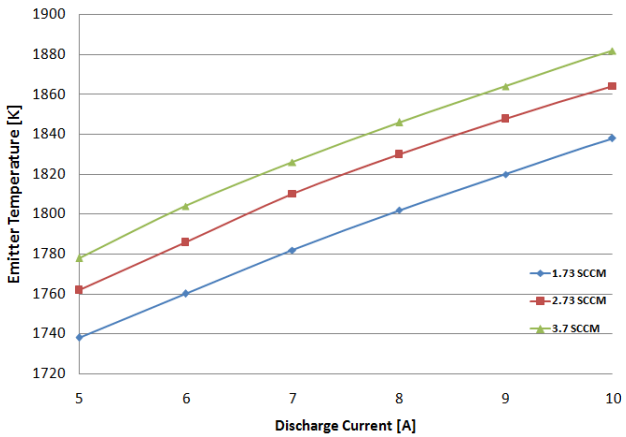


Figure 7: Insert wall temperature as a function of discharge current

The plasma density in the emitter region is plotted in Figure 8. The number density of the emitter plasma increases with increasing discharge current as experimentally shown by Jameson [22].

As was the case for emitter, it is found that the orifice plasma density is also an increasing function

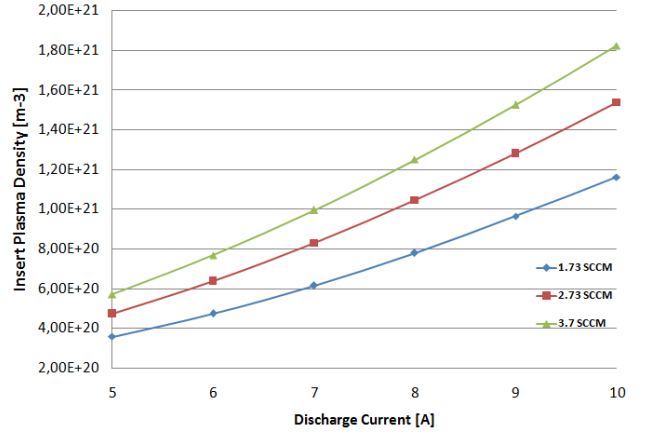


Figure 8: Emitter plasma density as a function of discharge current

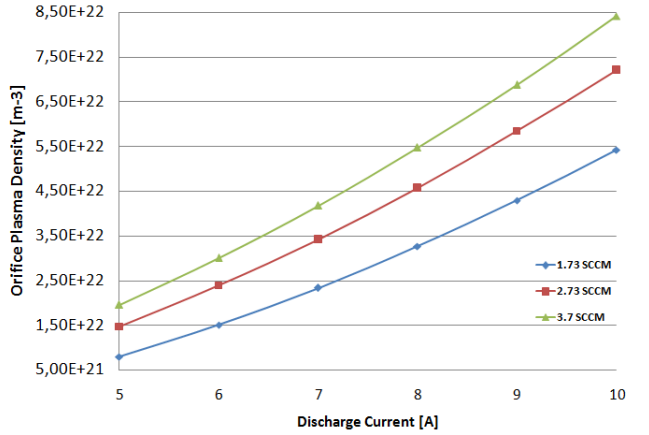


Figure 9: Orifice plasma density as a function of discharge current

of both discharge current and mass flow rate as seen in Figure 9.

The electron temperature of the orifice region is found to increase with discharge current whereas it decreases with the propellant flow rate as shown in Figure 10.

At 1.73 sccm xenon flow rate and 10 A discharge current, the influence of the geometry on the cathode has been also studied. According to Figure 11, the insert temperature is a decreasing function of the insert inner diameter. Another finding from the model is that the wall temperature of the insert decreases with the orifice diameter as seen in Figure 12. Larger orifice length causes a local power deposition in the orifice as a consequence the heat conduction from orifice toward the thermionic insert material enhances. In other words orifice heating becomes an important insert heating mechanism. This behaviour of hollow cathodes is captured in the present model as shown in Figure 13.

Lifetime of insert with respect to orifice length is also given in Figure 14. Heat conduction from ori-

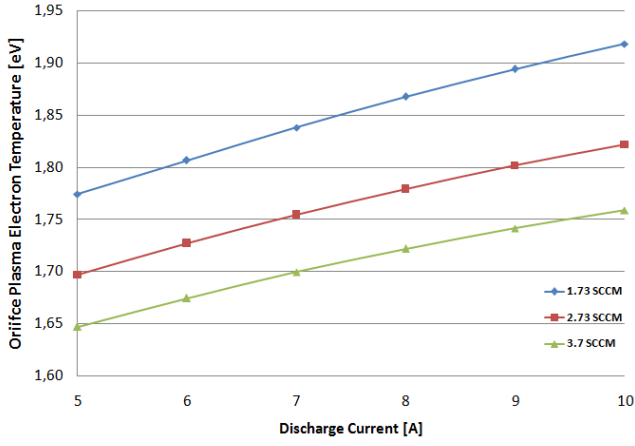


Figure 10: Orifice electron temperature as a function of discharge current

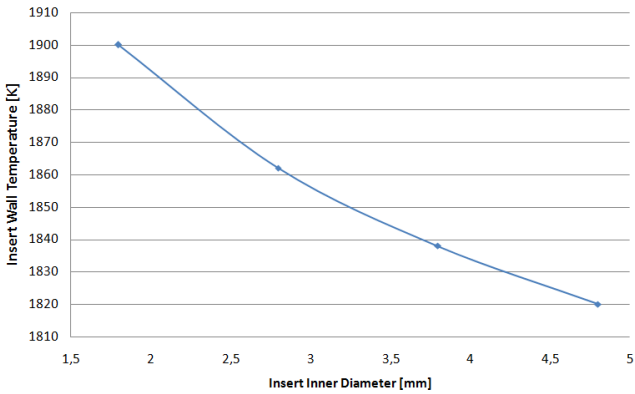


Figure 11: Insert temperature as a function of insert inner diameter

temperature to insert increases with increasing orifice length. As a result, insert lifetime decreases with increasing orifice length.

V. Conclusions

A volume-averaged model for orifice and insert regions of a typical orificed hollow cathode working with LaB₆ thermionic emitter was developed. Even though this model does not consider the spatial distributions of the particles in plasma, the results are encouraging for using it as a guideline for designing more efficient and longer life time hollow cathodes. The model can capture the effect of geometry and operation conditions on emitter and orifice regions. On the other hand, results of the present model needs to be compared with experimental and other theoretical models in order to verify that it is a reliable modelling tool for hollow cathodes.

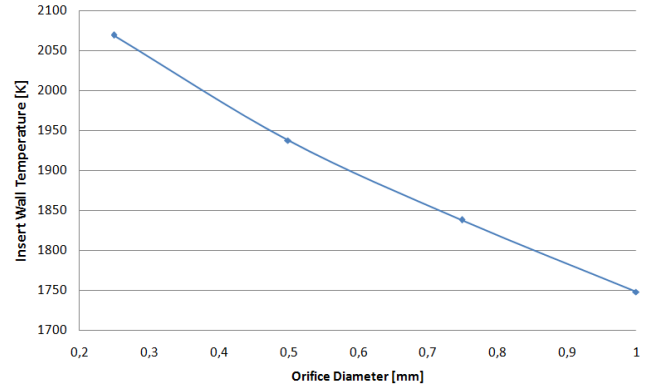


Figure 12: Insert temperature as a function of orifice diameter

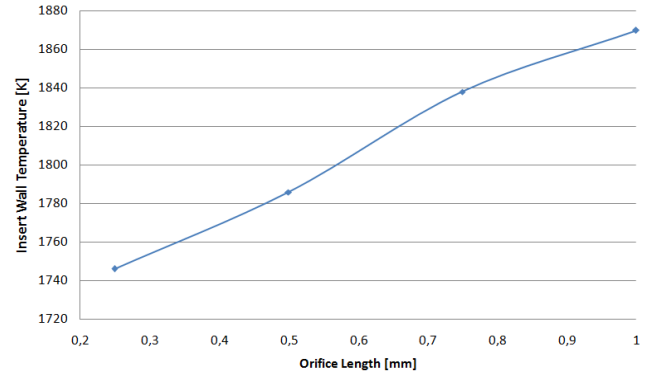


Figure 13: Insert wall temperature as a function of orifice length

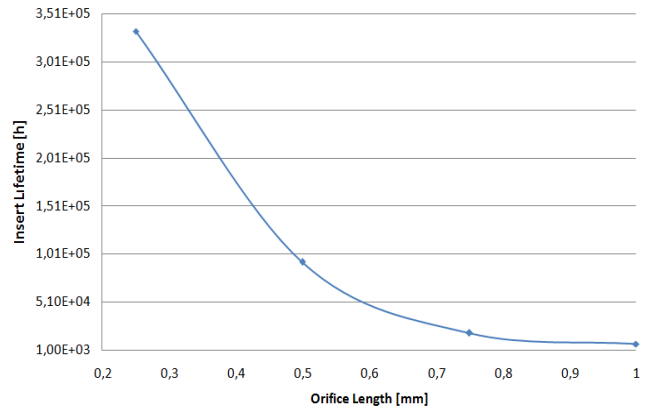


Figure 14: Insert lifetime as a function of orifice length

Acknowledgement

Authors would like to thank Ali Enes Ozturk for his valuable contribution to this study. This research is supported by Turkish Scientific and Technological Research Council (TUBITAK) under projects 112M862 and 113M244 and partially by Bogazici University Scientific Projects Office under project number BAP-6184.

References

- [1] Lafferty, J. M., “Boride Cathodes,” *Journal of Applied Cathodes*, Vol. 22, No. 3, 1951.
- [2] Goebel, D. M., Crow, J., and Forrester, A., “Lanthanum Hexaboride Hollow Cathode for Dense Plasma Production,” *Review of Scientific Instruments*, Vol. 49, No. 4, 2008, pp. 469–472.
- [3] Goebel, D. M. and Watkins, R. M., “Compact Lanthanum Hexaboride Hollow Cathode,” *Review of Scientific Instruments*, Vol. 81, No. 083504, 2010.
- [4] D. M. Goebel, R. M. W. and Jameson, K., “LaB₆ Hollow Cathodes for Ion and Hall Thrusters,” *AIAA Journal of Propulsion and Power*, Vol. 23, No. 3, 2010, pp. 527 – 528.
- [5] D. M. Goebel, Y. H. and Sketchley, T., “Large Area Lanthanum Hexaboride Electron Emitter,” *Review of Scientific Instruments*, Vol. 56, 1985, pp. 1717 – 1722.
- [6] Polk, J., Grubisic, A., Taheri, N., Goebel, D., Downey, R., and Hornbeck, S., “Emitter Temperature Distributions in the NSTAR Discharge Hollow Cathode,” *41th Joint Propulsion Conference*, Tucson, Arizona, USA, July 2005.
- [7] Mikellides, I. G., Katz, I., Goebel, D. M., and Polk, J. E., “Hollow Cathode Theory and Experiment. II. A Two-dimensional Theoretical Model of the Emitter Region,” *Journal of Applied Physics*, Vol. 98, No. 113303, 2005.
- [8] Goebel, D. M. and Katz, I., *Fundamentals of Electric Propulsion: Ion and Hall Thrusters*, JPL Space Science and Technology Series, New York, USA, 2008.
- [9] Coletti, M., Intini Marques, R., and Gabriel, S., “Discharge hollow cathode design for a 4-Gridded ion Engine,” *IEEE Aerospace Conference*, IEEE, 2010, pp. 1–12.
- [10] Domonkos, M. T., “Evaluation of Low-Current Orificed Hollow Cathodes,” Ph.D. Thesis, The University of Michigan, Ann Arbor, MI, 1999.
- [11] I. Katz, M. J. Mandell, M. P. and Domonkos, M., “Sensitivity of Hollow Cathode Performance to Design and Operating Parameters,” *35th Joint Propulsion Conference and Exhibit*, Los Angeles, CA, USA, June 1999, AIAA-1999-2576.
- [12] Crawford, F. W. and Freeston, I. L., “The Double Sheath at a Discharge Constriction,” *6th International Conference on Ionization Phenomena in Gases*, Paris, July 1963, V.1 pp. 461-464.
- [13] D. M. Goebel, K. K. Jameson, R. M. W. and Katz, I., “Hollow cathode and keeper-region plasma measurements using ultra-fast miniature scanning probes,” *40th Joint Propulsion Conference and Exhibit*, AIAA, July 2007.
- [14] Siegfried, D. E. and Wilbur, P. J., “An Investigation of Mercury Hollow Cathode Phenomena,” *13th International Electric Propulsion Conference*, San Diego, CA, USA, April 25-27 1978, AIAA 1978-705.
- [15] I. Katz, I. G. Mikellides, D. M. G. J. E. P., “Insert heating and ignition in inert-gas hollow cathodes,” *IEEE Transactions on Plasma Science*, Vol. 36, No. 5, 2008, pp. 2199–2206.
- [16] Chu, E. and Goebel, D. M., “High-current lanthanum hexaboride hollow cathode for 10-to-50-kW Hall thrusters,” *IEEE Transactions on Plasma Science*, Vol. 40, No. 9, 2012, pp. 2133–2144.
- [17] R. Albertoni, D. Pedrini, F. P. and Andrenucci, M., “A Reduced Order Model For Thermionic Hollow Cathodes,” *IEEE Transactions on Plasma Science*, Vol. 43, No. 7, 2013, pp. 1731–1745.
- [18] Domonkos, M. T., “A Particle and Energy Balance Model of the Orificed Hollow Cathode,” *38th Joint Propulsion Conference*, Indianapolis, USA, July 2002, AIAA-2002-4240.
- [19] D. M. Goebel, C. E., “High Current Lanthanum Hexaboride Hollow Cathodes for High Power Hall Thrusters,” *32nd International Electric Propulsion Conference*, Weisbaden, Germany, September 2011.
- [20] Salhi, A., “Theoretical and Experimental Studies of Orificed, Hollow Cathode Operation,” Ph.D. Dissertation, Ohio State University, Columbus, OH, USA, 1993.
- [21] Goebel, D., Jameson, K. K., and Hofer, R. R., “Hall Thruster Cathode Flow Impact on Coupling Voltage and Cathode Life,” *Journal of Propulsion and Power*, Vol. 28, No. 2, 2012, pp. 355–363.
- [22] K. K. Jameson, D. M. G. and Watkins, R. M., “Hollow Cathode and Thruster Discharge Chamber Plasma Measurements Using High-Speed Scanning Probes,” *29th IEPC*, Princeton, NJ, USA, October 2005.